Carbon Nanotubes

DOI: 10.1002/ange.201402258

# Mechanically Interlocked Single-Wall Carbon Nanotubes**

*Alberto de Juan, Yann Pouillon, Luisa Ruiz-González, Almudena Torres-Pardo, Santiago Casado, Nazario Martín, Ángel Rubio, and Emilio M. Pérez**

***Abstract:*** *Extensive research has been devoted to the chemical manipulation of carbon nanotubes. The attachment of molecular fragments through covalent-bond formation produces kinetically stable products, but implies the saturation of some of the C–C double bonds of the nanotubes. Supramolecular modification maintains the structure of the SWNTs but yields labile species. Herein, we present a strategy for the synthesis of mechanically interlocked derivatives of SWNTs (MINTs). In the key rotaxane-forming step, we employed macrocycle precursors equipped with two π-extended tetrathiafulvalene SWNT recognition units and terminated with bisalkenes that were closed around the nanotubes through ring-closing metathesis (RCM). The mechanically interlocked nature of the derivatives was probed by analytical, spectroscopic, and microscopic techniques, as well as by appropriate control experiments. Individual macrocycles were observed by HR STEM to circumscribe the nanotubes.*

Ever since their discovery,[1] carbon nanotubes have remained in the spotlight of physical and chemical research owing to their outstanding physical properties.[2] However, the initial excitement about their possible application in the field of organic electronics has only recently started to become a reality.[3] The contribution of chemistry to carbon-nanotube science is focused on their synthesis,[4] and their covalent[5] or noncovalent[6] modification to attain specific electronic properties. The covalent modification of single-wall nanotubes (SWNTs) provides kinetically stable products, but implies the saturation of some of the C–C double bonds of the nanotubes. The supramolecular modification of SWNTs enables conservation of the structure of the nanotubes, but in most cases the products lack kinetic stability.[7]

A hitherto unexplored alternative is to modify the SWNTs to form mechanically interlocked species.[8] Mechanically interlocked molecules (MIMs) consist of two or more separate components which are not connected by chemical (i.e. covalent) bonds. Examples of MIMs are rotaxanes, in which one or more macrocycles are trapped on a linear component (thread) by bulky substituents at its ends (stoppers) that prevent dissociation, and catenanes, in which two or more macrocycles are interlocked in the same way as links in a chain. Owing to their unique dynamic properties, MIMs have been extensively studied as candidates for the construction of synthetic molecular machinery.[9] For example, self-assembled monolayers of molecular shuttles—rotaxanes in which the macrocycle can be moved between two or more sites on the thread in response to external stimuli—are able to produce mechanical work[10] and to store information.[11] Recently, multistation molecular shuttles have been shown to perform sequence-specific peptide synthesis,[12] thus imitating one of the most complex pieces of naturally existing molecular machinery, the ribosome. Besides the application of MIMs to the synthesis of molecular machinery, the encapsulation of elongated molecules to form kinetically stable rotaxanes has been proven to give rise to a variety of novel properties. As a consequence, there is growing interest in the production of mechanically interlocked hybrid materials, such as polymers[13] and metal–organic frameworks.[14] The 1D structure of SWNTs opens up the possibility of utilizing them as threads in the synthesis of rotaxane-type mechanically interlocked nanotubes (MINTs).[15] To the best of our knowledge, this possibility has only been studied from a theoretical point of view.[16] Herein, we describe the synthesis of rotaxanes in which SWNTs act as threads.

Given the structural similarities between fullerenes and SWNTs, we based our design on our previous experience in the synthesis of macrocyclic receptors for fullerenes.[17] Macrocycles **1**–**3** (Figure 1 a) feature two π-extended tetra-

[*] A. de Juan, Dr. S. Casado, Prof. Dr. N. Martín, Dr. E. M. Pérez
IMDEA Nanoscience, C/Faraday 9
Ciudad Universitaria de Cantoblanco
28049 Madrid (Spain)
E-mail: emilio.perez@imdea.org
Dr. Y. Pouillon, Prof. Dr. Á. Rubio
European Theoretical Spectroscopy Facility, Centro Joxe Mari Korta
Avenida de Tolosa, 72, 20018 Donostia-San Sebastian (Spain)
Dr. L. Ruiz-González, Dr. A. Torres-Pardo
Departamento de Química Inorgánica, Fac. C.C. Químicas
Universidad Complutense de Madrid
Avenida Complutense s/n, 28040 Madrid (Spain)

[**] We thank Dr. D. B. M. Walker for useful comments on the original version of the manuscript. A.d.J and E.M.P. are grateful for funding from the European Research Council (Starting Independent Research Grant MINT; ERC-2012-StG Proposal No. 307609) and the Spanish MINECO (CTQ2011-25714). N.M. acknowledges funding from the Spanish MINECO (CTQ2011-24652) and the Comunidad Autónoma de Madrid (MADRISOLAR-2 S2009/PPQ-1533). Y.P. and A.R. acknowledge funding from the European Research Council (Advanced Grant DYNamo; ERC-2010-AdG Proposal No. 267374), CRONOS (Grant number 280879-2 CRONOS CP-FP7), POCAONTAS (FP7-PEOPLE-2012-ITN-Project 316633), and the Spanish Grants FIS2010-21282-C02-01, as well as the "Grupos Consolidados UPV/EHU del Gobierno Vasco" (IT-578-13). A.T.-P. was supported by a PICATA postdoctoral fellowship of the Moncloa Campus of International Excellence (UCM). We thank Prof. José M. González, director of the National Center for Electron Microscopy (CNME; UCM, Madrid), for facilities and valuable scientific advice on the JEOL-JSM-ARM200F microscope, which was recently installed and tuned up in the CNME.

Supporting information for this article is available on the WWW under http://dx.doi.org/10.1002/anie.201402258.

  

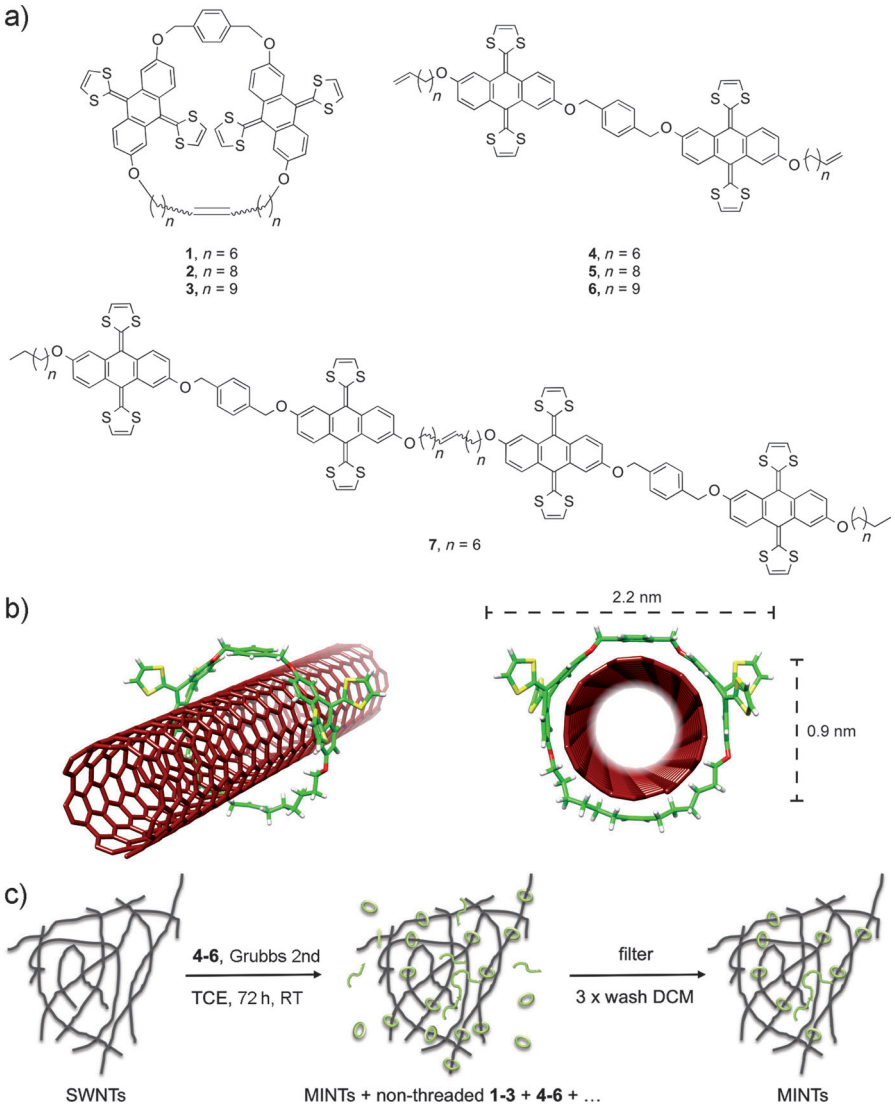


***Figure 1.*** a) Chemical structure of macrocycles **1**–**3** and their linear precursors **4**–**6**. The structure of linear oligomer **7** is also shown. b) Energy-minimized (MMFF94) molecular model of a pseudorotaxane comprising **1** and a (7,6) SWNT. Carbon atoms of the macrocycle are shown in green, sulfur in yellow, oxygen in red, and hydrogen in white. Carbon atoms of the SWNT are shown in dark red. The diameters of the nanotube and macrocycle **1** are also shown. c) Schematic representation of the RCM clipping reaction and purification procedure, as based on experimental data (see main text). Note that some longer oligomers/polymers might also form part of the MINT mixture.

thiafulvalene (9,10-di(1,3-dithiol-2-ylidene)-9,10-dihydroanthracene, exTTF) units, which have been previously shown to serve as a recognition motif for SWNTs.[18] The recognition units are linked together through 1,4-xylylene and $C_{14}$, $C_{18}$, or $C_{20}$ alkenyl spacers. The macrocycles were synthesized by ring-closing metathesis (RCM) of the corresponding linear precursors **4**–**6** (Figure 1a). To investigate the required diameter for a SWNT to be appropriate for threading through macrocycle **1**, as a model system, we carried out an extensive theoretical search, in which the association of **1** with as many as 40 different SWNT chiralities was modeled. To that end, we chose the relatively inexpensive MMFF94 force field, which is known to provide satisfactory structural accuracy for a broad range of systems, including SWNTs. For one case, a (12,0) SWNT with **1**, we compared the force-field geometry to that obtained from a DFT calculation and found no significant difference (see Computational Details in the Supporting Information). On the basis of these calculations, we estimated that **1** was able to encapsulate SWNTs of diameters smaller than 0.91 nm with significantly positive interaction energy. Among the SWNT configurations investigated, (6,5), (7,5), (7,6), (8,4), (8,5), and (9,4) nanotubes showed the highest predicted binding energies, between 29.6 and 166.9 kJ mol$^{-1}$ (see Table S1 in the Supporting Information). The energy-minimized structure of a pseudorotaxane comprising **1** and a (7,6) SWNT is shown in Figure 1b.

Considering the results of the calculations, in a first attempt we utilized (7,6)-enriched SWNTs purchased from Sigma-Aldrich (0.7–1.1 nm in diameter, 90% purity after purification). The nanotubes (20 mg) were suspended in tetrachloroethane (TCE; 20 mL) through sonication and mixed with linear precursor **4** (10 mg, 0.0087 mmol) and Grubbs' second-generation catalyst at room temperature for 72 h. We expected the nanotube to serve as a template for the macrocycle, which would be formed around it (Figure 1c). We relied on RCM, since the fully substituted $sp^2$ carbon atoms of the SWNT are unlikely to react under these conditions.[19] After this time, the suspension was filtered through a polytetrafluoroethylene membrane with a pore size of 0.2 μm, and the solid was washed profusely with $CH_2Cl_2$ to remove nonthreaded macrocycles, catalyst, and any remaining linear precursor. Thermogravimetric analysis (TGA) of the solid thus obtained showed a weight loss of 37% at approximately 400°C (Figure 2a). When the same reaction was carried out with plasma-purified SWNTs purchased from Cheap Tubes Inc. (0.8–1.6 nm in diameter, 99% purity), the product obtained showed a weight loss of 29% (Figure 2b), in accordance with a smaller ratio of SWNTs with diameters suitable for encapsulation with **1**. The diameter of the macrocycle also affects the degree of functionalization. For example, when the reaction was carried out with linear precursor **5** or **6** instead of **4**, under otherwise identical experimental conditions, TGA analysis showed 23 and 31% weight loss, respectively (see Figure S1 in the Supporting Information). This high loading of exTTF mate-

  

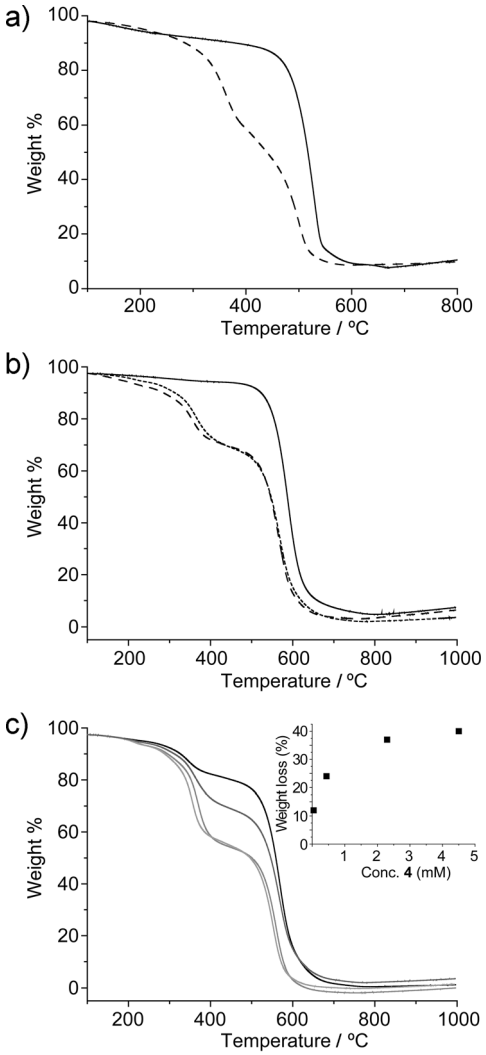


***Figure 2.*** a) TGA analysis (air, 10 °C min$^{-1}$) of pristine (7,6)-enriched SWNTs (solid line) and the product formed by treatment with **4** (10 mg, 0.0087 mmol) and the Grubbs second-generation catalyst in TCE (20 mL) at room temperature for 72 h (dashed line). b) TGA analysis (air, 10 °C min$^{-1}$) of pristine plasma-purified SWNTs (solid line), the product formed by treatment with **4** (10 mg, 0.0087 mmol) and the Grubbs second-generation catalyst in TCE (20 mL) at room temperature for 72 h (dotted line), and the same sample after heating at reflux in TCE for 30 min and filtration (dashed line, showing the stability of the noncovalent modification). c) Variation in the degree of functionalization with the relative concentration of **4** with respect to that of the SWNTs, as shown by TGA analysis (air, 10 °C min$^{-1}$): 0.044 mM (black), 0.44 mM (dark gray), 2.3 mM (gray), and 4.5 mM (light gray). Inset shows the relative weight loss versus the concentration of **4**.

rial suggests that, besides encapsulation by macrocycles **1**–**3**, other types of functionalization of the nanotubes, by oligomers or higher-order macrocycles formed in situ from the linear precursors, may also make a significant contribution. Functionalization by linear oligomers should be completely diameter-independent, so the dependence of the amount of exTTF material attached to the SWNTs on the size of the cavity of the macrocycle and the diameter of the nanotubes indicates that this type of functionalization plays a minor role.[20] In support of this hypothesis, HPLC analysis of the filtrate of the clipping reaction of **4** around the plasma-purified SWNTs showed macrocycle **1** and the unreacted linear precursor only, in a 64:36 **4**/**1** ratio. In comparison, analysis of an identical RCM reaction carried out in the absence of SWNTs showed a very similar HPLC trace, but with a 47:53 **4**/**1** ratio, which shows that a significant amount of **1** was retained in the SWNT material (see Figure S2 in the Supporting Information). No oligomers of **4** were detected. All these data indicate that encapsulation of the nanotubes by **1**–**3** or, to some extent, higher-order macrocycles is the major type of functionalization. Both would lead to the desired interlocked species. Nevertheless, owing to the intrinsically heterogeneous nature of the sample, the possibility of a certain degree of functionalization by oligomers/polymers cannot be fully discarded.

By varying the relative concentration of **4** with respect to SWNTs we could modulate the degree of functionalization. We performed experiments with the plasma-purified SWNTs in which the concentration of **4** was decreased by a factor of ten (0.044 mM) and increased by factors of five (2.3 mM) and ten (4.5 mM) with respect to the original experiment (0.44 mM). TGA analysis of these samples is shown in Figure 2c. The product formed with the lowest concentration of **4** showed a loss of 12% at 400 °C, whereas a weight loss of 35 or 37% was observed when the concentration of **4** was increased by a factor of five and ten, respectively. These data clearly show that the degree of functionalization does not have a linear relationship with the concentration of **4**, but instead reaches a maximum at about 40%, which corresponds approximately to one macrocycle for every 140 nanotube carbon atoms (Figure 2c, inset).

This degree of functionalization was maintained even after three consecutive washes, in which the sample was resuspended in $CH_2Cl_2$ (20 mL), sonicated (10 min), and filtered, thus indicating that there is little or no exchange between bound and unbound macrocycles. Even heating at reflux in tetrachloroethane (b.p. = 147 °C; 30 min), followed by a thorough rinse with $CH_2Cl_2$, did not lead to a significant loss of loading (Figure 2b). In fact, the only way in which the macrocycles could be removed was through calcination of the sample at 360 °C for 30 min (see Figure S3 in the Supporting Information).

We reasoned that, besides the high affinity of the macrocycles for SWNTs, this outstanding stability could originate from a high energy barrier for the dethreading process, most likely as a result of the formation of cross-points, which would act as stoppers, between the nanotubes (Figure 1c). To test this hypothesis, we carried out the clipping reaction with shorter, but otherwise identical, plasma-purified nanotubes (0.2–5 μm versus 3–30 μm), which should be less likely to form cross-points. TGA analysis of the product showed a functionalization of 20%, a significant decrease with respect to the original 29% observed for the longer tubes (see Figure S4 in the Supporting Information). Moreover, we also attempted the direct encapsulation of a suspension of the long plasma-purified SWNTs (20 mg) in TCE (20 mL) by stirring with macrocycle **1** (10 mg, 0.0089 mmol) for 72 h at room temper-

ature. The resulting product was analyzed by TGA, which showed a weight loss of only 7% (see Figure S5 in the Supporting Information); this low weight loss indicates that the threading process is indeed highly unlikely.

Since some residual functionalization was still observed, we decided to quantify the direct association of **4** with the walls of the SWNTs by mixing **4** (10 mg, 0.0087 mmol) and SWNTs (20 mg) in TCE (20 mL) in the absence of the RCM catalyst. Similarly to the previous experiment, we observed a weight loss of around 6% by TGA (see Figure S6 in the Supporting Information). This value suggests that both products are the result of the adsorption of either **1** or **4** on the sidewalls of the SWNTs. An increase in the number of exTTF units to four, with linear dimer **7**, led to a slight increase in the amount of material attached to the SWNTs (9% weight loss in TGA at the same temperature; see Figure S7 in the Supporting Information), thus providing further evidence that functionalization by oligomers plays a minor role only.

To characterize our MINT samples, we carried out solid-state cross-polarization magic-angle spinning (CP MAS) $^{13}$C NMR spectroscopy, UV/Vis/NIR spectroscopy, photoluminescence excitation intensity mapping (PLE), and Raman spectroscopy, all of which were in agreement with the noncovalent functionalization of the SWNTs with **1**. The CP MAS $^{13}$C NMR spectrum of the mechanically interlocked sample of the plasma-purified nanotubes, MINT$_{pp}$-**1**, showed signals in the $\delta = 150$–100, 80–60, and 40–20 ppm regions, which were assigned to the sp$^2$-hybridized nanotube carbon atoms plus the aromatic atoms of **1**, the alkene moieties, and the alkyl spacers of **1**, respectively. For comparison, the CP MAS $^{13}$C NMR spectrum of **1** was also recorded and showed much better defined signals in similar areas of the spectrum. The relative integrals of the aromatic/alkene/alkyl regions in **1** are approximately 2.6:0.2:1.0, whereas in MINT$_{pp}$-**1** they are 4.7:0.2:1.0, thus showing that the nanotube carbon atoms are cross-polarized via the hydrogen atoms of the macrocycle. In contrast, neither the pristine nanotubes nor the products of the control experiments without the Grubbs catalyst or with the preformed macrocycle **1** showed any signals (Figure 3a). The UV/Vis/NIR spectra of pristine (7,6)-enriched SWNTs and the corresponding MINT$_{(7,6)}$-**1** sample are shown in Figure 3b. The absorption spectra of the SWNTs shows features in the $M_{11}$, $S_{22}$, and $S_{11}$ regions of the spectra, with the absorption of the (7,6) nanotube clearly distinguishable at $\lambda = 650$ and 1120 nm.[21] Upon derivatization, these bands are significantly shifted bathochromically, to $\lambda = 660$ and 1150 nm, respectively. Most other absorption bands in the $S_{11}$ and $S_{22}$ regions of the spectra are also shifted to a similar extent.

In the PLE experiments (Figure 4), SWNTs of configurations (6,5), (7,5), (7,6), (8,4), and (9,4) were detected in the (7,6)-enriched sample, all of which should present significant positive interactions with **1** according to our calculations. Upon the formation of MINT$_{(7,6)}$-**1**, their luminescence is significantly quenched and red-shifted, as could be expected. For example, in the case of the (7,6) tubes, as compared to a sample of pristine SWNTs of the same optical density, the excitation is shifted from 644 to 648 nm, and the emission is shifted from 1142 to 1152 nm and quenched to approximately half the intensity.

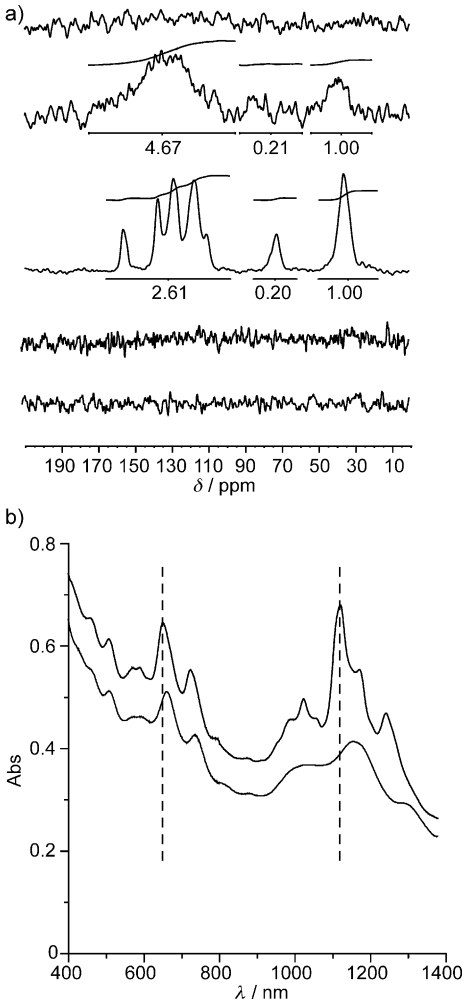


***Figure 3.*** a) CP MAS $^{13}$C NMR spectra of (from top to bottom): pristine plasma-purified SWNTs, MINT$_{pp}$-**1**, macrocycle **1**, SWNTs after treatment with **4**, and SWNTs after treatment with **1**. b) UV/Vis/NIR spectra ($D_2O$, 1% sodium dodecyl sulfate (SDS), 298 K) of pristine (7,6)-enriched SWNTs (top, black) and MINT$_{(7,6)}$-**1** (bottom, gray). The absorption features of the (7,6) nanotube are marked with a vertical dashed line.

The Raman spectra of as-purchased plasma-purified SWNTs and MINT$_{pp}$-**1** are compared in Figure 5a–c ($\lambda_{exc} =$ 785 nm). The two spectra are very similar, thus proving that the structure of the nanotubes is preserved upon modification, with no increase in the relative intensity of the D band. Meanwhile, the G band is shifted from 1576 cm$^{-1}$ in the pristine SWNT to 1577 cm$^{-1}$ in MINT$_{pp}$-**1** (Figure 5b). This small shift is in agreement with previous findings for the noncovalent modification of SWNTs with exTTF-based tweezers[18] and implies that there is no significant charge transfer from the electron-donor exTTF moiety to the SWNTs in the ground state. The change in the radial breathing modes (RBM) are also small. The signals at lower wave numbers (150–200 cm$^{-1}$), which correspond to SWNTs too large to be encapsulated by **1**, are unaltered, whereas those appearing between 250 and 300 cm$^{-1}$ (SWNT diameter:

  

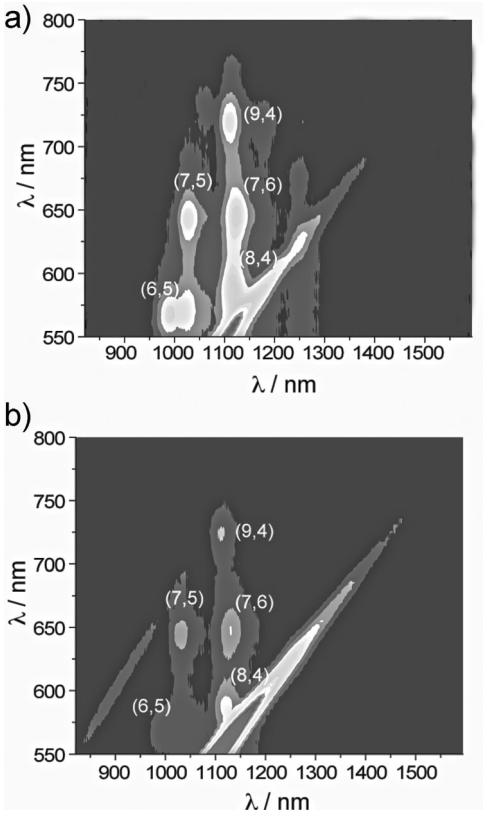


***Figure 4.*** PLE intensity maps ($D_2O$, 1% SDS, 298 K) of a) pristine (7,6)-enriched SWNTs and b) $MINT_{(7,6)}$-**1**. Intensities range from 0 to 1650 counts. Rayleigh scattering has not been filtered.

1–0.8 nm) are shifted to higher frequencies, for example, from 259 to 260 $cm^{-1}$. The shifts in the spectra of the (7,6)-enriched sample upon functionalization are very similar (Figure 5 d–f). The G band is shifted from 1585 to 1587 $cm^{-1}$, whereas the RBM of the (7,6) SWNT is shifted from 259 to 260 $cm^{-1}$. The modifications with green laser excitation follow the same trends (see Figure S8 in the Supporting Information). All these data are consistent with the modification of the nanotubes to form MINT-**1**.

The investigation of a sample of $MINT_{(7,6)}$-**1** under atomic force microscopy (AFM, dynamic mode) was also in agreement with the formation of the rotaxane-type species. Figure 6 a shows a topographic image of a single SWNT with a height of approximately 1 nm, on which three separate elevations of approximately 2.5 nm are observed. The dimensions and the regularity of these elevations are perfectly consistent with the formation of **1** around a SWNT (Figure 1 b). If either **1** or unreacted **4** were simply adsorbed on top of the SWNT, the vertical dimension would be significantly smaller (ca. 1.6 nm; see Figure S9 in the Supporting Information). The phase image (Figure 6 b) shows that there is higher energy diffusion at the protuberances, thus indicating that they are not nanotube inhomogeneities. In contrast, AFM images of the pristine SWNTs do not show protuberances of regular height nor differences in the phase channel (see Figure S10 in the Supporting Information).

Finally, transmission electron microscopy (TEM) provided conclusive support for the formation of MINTs. Pioneering studies by Nakamura and co-workers have offered extensive evidence of the observation of a variety of small organic molecules under TEM in the vicinity of carbon nanotubes.[22] An image of $MINT_{pp}$-**1** obtained under a JEOL-JEM 2100F microscope (2.5 Å resolution), like the microscope utilized by Nakamura and co-workers in their seminal study,[23] is shown in Figure 6 c. Most of the individual SWNTs show densely covered walls (Figure 6 c, white ellipse), in agreement with the high degree of functionalization determined by TGA, but we were pleased to observe that in numerous cases distinct circular objects could be detected around the nanotubes, in several different areas of the sample (Figure 6 c, white circles). The diameter of the nanotubes (ca. 1.4 nm) and of the macrocyclic components (ca. 4 nm) suggests that these circular objects are the result of a bimolecular macrocyclization of **4**. Figure 6 d shows a TEM image of the $MINT_{(7,6)}$-**1** sample, in which an isolated SWNT of diameter 0.8 nm surrounded by an object of an appropriate size to be **1** (ca. 2.2 nm) can be seen. To perform a more precise characterization, we also employed an aberration-corrected microscope. The microscope was operated at 80 kV to prevent damage to the nanotubes and

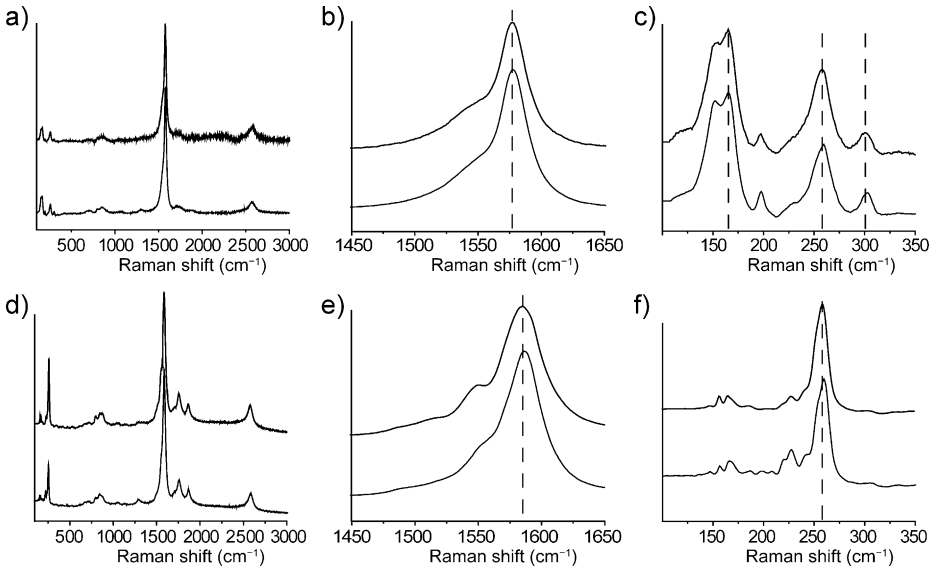


***Figure 5.*** a) Raman spectra ($\lambda_{exc} = 785$ nm) of plasma-purified SWNTs (top, black) and the corresponding $MINT_{pp}$-**1** (bottom, gray); b) magnification of the G zone; c) magnification of the RBM zone (dashed vertical lines have been added as a guide to the eye). d) Raman spectra of (7,6)-enriched SWNTs (top, black) and the corresponding $MINT_{(7,6)}$-**1** (bottom, gray); e) magnification of the G zone; f) magnification of the RBM zone. All spectra are the average of three different measurements.

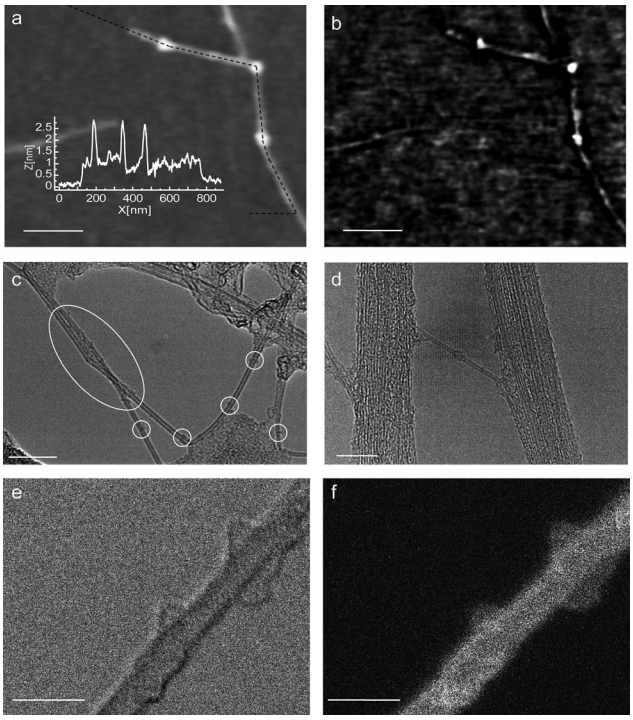


***Figure 6.*** a) AFM topographic image of a spin-cast suspension of $MINT_{(7,6)}$-**1** in TCE. The inset shows the profile along the dashed black line. b) Phase image of the area shown in (a). c) TEM image of nanotubes (showing a densely covered surface) and several individual macrocycles in the $MINT_{pp}$-**1** sample. d) TEM image of an individual SWNT in the $MINT_{(7,6)}$-**1** sample; the image shows an object of appropriate dimensions to be **1**. e) HR STEM bright-field image of a single SWNT surrounded by two macrocycles in the $MINT_{(7,6)}$-**1** sample. f) HR STEM dark-field image of the same nanotube. Scale bars are 100 nm for (a,b), 20 nm for (c), 10 nm for (d), and 2 nm for (e,f).

macrocycles. Under these working conditions, in scanning transmission electron (STEM) mode, a spatial resolution of 1.1 Å is guaranteed. Figure 6e,f shows the bright-field and dark-field high-resolution (HR) STEM images, recorded simultaneously, of the $MINT_{(7,6)}$-**1** sample. In the bright-field image, a single SWNT of 0.8 nm in diameter and functionalized with two separate macrocycles can be observed. The macrocycles are again commensurate with **1** in terms of their size (ca. 2.2 nm). The dark-field image shows a similar contrast for the macrocycles and the SWNT, in accordance with their composition. Energy-dispersive X-ray spectroscopy (EDX) of the MINT-**1** samples confirmed the presence of a significant amount of sulfur (ca. 1%), in good agreement with the TGA data (see Figure S11 in the Supporting Information).

In conclusion, we have introduced the mechanical bond as a new tool for the chemical manipulation of SWNTs. Our synthetic approach is based on a clipping strategy in which the macrocycles are formed around the SWNTs by RCM. Once in place, the macrocycles remained attached to the nanotubes even after reflux in TCE for 30 min, and could only be removed by calcination at 360°C. Raman spectroscopy showed that the changes to the electron–phonon structure of the SWNTs upon formation of the mechanically interlocked species are small, and comparable to those observed after typical noncovalent modification. PLE maps suggest that a charge-transfer process occurs from the donor exTTF unit to the nanotubes upon photoexcitation. We now intend to extend this strategy to other types of macrocycles and to investigate the properties of the MINTs exhaustively.

Received: February 11, 2014
Published online: April 11, 2014

**Keywords:** nanotubes · π interactions · ring-closing metathesis · rotaxanes · supramolecular chemistry

[1] a) S. Iijima, T. Ichihashi, *Nature* **1993**, *363*, 603–605; b) S. Iijima, *Nature* **1991**, *354*, 56–58; c) D. S. Bethune, C. H. Kiang, M. S. de Vries, G. Gorman, R. Savoy, J. Vazquez, R. Beyers, *Nature* **1993**, *363*, 605–607.

[2] a) R. H. Baughman, A. A. Zakhidov, W. A. de Heer, *Science* **2002**, *297*, 787–792; b) K. Dirian, M. Á. Herranz, G. Katsukis, J. Malig, L. Rodríguez-Pérez, C. Romero-Nieto, V. Strauss, N. Martín, D. M. Guldi, *Chem. Sci.* **2013**, *4*, 4335–4353.

[3] a) A. D. Franklin, M. Luisier, S.-J. Han, G. Tulevski, C. M. Breslin, L. Gignac, M. S. Lundstrom, W. Haensch, *Nano Lett.* **2012**, *12*, 758–762; b) H. Park, A. Afzali, S.-J. Han, G. S. Tulevski, A. D. Franklin, J. Tersoff, J. B. Hannon, W. Haensch, *Nat. Nanotechnol.* **2012**, *7*, 787–791.

[4] For reviews, see: a) H. Dai, *Acc. Chem. Res.* **2002**, *35*, 1035–1044; b) M. C. Hersam, *Nat. Nanotechnol.* **2008**, *3*, 387–394; c) W. Zhou, X. Bai, E. Wang, S. Xie, *Adv. Mater.* **2009**, *21*, 4565–4583; d) R. Jasti, C. R. Bertozzi, *Chem. Phys. Lett.* **2010**, *494*, 1–7; e) Y. Zhang, L. Zheng, *Nanoscale* **2010**, *2*, 1919–1929; for recent examples, see: f) H. Omachi, T. Nakayama, E. Takahashi, Y. Segawa, K. Itami, *Nat. Chem.* **2013**, *5*, 572–576; g) H. Kimura, J. Goto, S. Yasuda, S. Sakurai, M. Yumura, D. N. Futaba, K. Hata, *ACS Nano* **2013**, *7*, 3150–3157; h) L. T. Scott, E. A. Jackson, Q. Zhang, B. D. Steinberg, M. Bancu, B. Li, *J. Am. Chem. Soc.* **2012**, *134*, 107–110.

[5] P. Singh, S. Campidelli, S. Giordani, D. Bonifazi, A. Bianco, M. Prato, *Chem. Soc. Rev.* **2009**, *38*, 2214–2230.

[6] Y.-L. Zhao, J. F. Stoddart, *Acc. Chem. Res.* **2009**, *42*, 1161–1171.

[7] For kinetically stable supramolecular derivatives through interaction with oligomers/polymers, see: a) J. Gao, M. A. Loi, E. J. F. de Carvalho, M. C. dos Santos, *ACS Nano* **2011**, *5*, 3993–3999; b) A. Llanes-Pallas, K. Yoosaf, H. Traboulsi, J. Mohanraj, T. Seldrum, J. Dumont, A. Minoia, R. Lazzaroni, N. Armaroli, D. Bonifazi, *J. Am. Chem. Soc.* **2011**, *133*, 15412–15424; c) S. D. Stranks, J. K. Sprafke, H. L. Anderson, R. J. Nicholas, *ACS Nano* **2011**, *5*, 2307–2315; through interaction with DNA: d) Y. Liu, Z.-L. Yu, Y.-M. Zhang, D.-S. Guo, Y.-P. Liu, *J. Am. Chem. Soc.* **2008**, *130*, 10431–10439; e) X. Tu, S. Manohar, A. Jagota, M. Zheng, *Nature* **2009**, *460*, 250–253; f) F. D'Souza, S. K. Das, M. E. Zandler, A. S. D. Sandanayaka, O. Ito, *J. Am. Chem. Soc.* **2011**, *133*, 19922–19930; for other examples, see: g) H. Chaturvedi, A. N. Giordano, M.-J. Kim, F. M. MacDonnell, S. S. Subaran, J. C. Poler, *J. Phys. Chem. C* **2009**, *113*, 11254–11261; h) G. Clavé, G. Delport, C. Roquelet, J.-S. Lauret, E. Deleporte, F. Vialla, B. Langlois, R. Parret, C. Voisin, P. Roussignol, B. Jousselme, A. Gloter, O. Stephan, A. Filoramo, V. Derycke, S. Campidelli, *Chem. Mater.* **2013**, *25*, 2700–2707.

[8] a) J. F. Stoddart, *Chem. Soc. Rev.* **2009**, *38*, 1802–1820; b) J.-P. Sauvage, *Chem. Commun.* **2005**, 1507–1510.

[9] E. R. Kay, D. A. Leigh, F. Zerbetto, *Angew. Chem.* **2007**, *119*, 72–196; *Angew. Chem. Int. Ed.* **2007**, *46*, 72–191.

[10] J. Berná, D. A. Leigh, M. Lubomska, S. Mendoza, E. M. Pérez, P. Rudolf, G. Teobaldi, F. Zerbetto, *Nat. Mater.* **2005**, *4*, 704–710.

  

[11] J. E. Green, J. W. Choi, A. Boukai, Y. Bunimovich, E. Johnston-Halperin, E. DeIonno, Y. Luo, B. A. Sheriff, K. Xu, Y. S. Shin, H.-R. Tseng, J. F. Stoddart, J. R. Heath, *Nature* **2007**, *445*, 414 – 417.
[12] B. Lewandowski, G. De Bo, J. W. Ward, M. Papmeyer, S. Kuschel, M. J. Aldegunde, P. M. E. Gramlich, D. Heckmann, S. M. Goldup, D. M. D'Souza, A. E. Fernandes, D. A. Leigh, *Science* **2013**, *339*, 189 – 193.
[13] L. Fang, M. A. Olson, D. Benítez, E. Tkatchouk, W. A. Goddard III, J. F. Stoddart, *Chem. Soc. Rev.* **2010**, *39*, 17 – 29.
[14] Q. Li, C.-H. Sue, S. Basu, K. S. Alexander, W. Zhang, G. Barin, L. Fang, A. S. Amy, J. F. Stoddart, M. Y. Omar, *Angew. Chem.* **2010**, *122*, 6903 – 6907; *Angew. Chem. Int. Ed.* **2010**, *49*, 6751 – 6755.
[15] A. de Juan, E. M. Pérez, *Nanoscale* **2013**, *5*, 7141 – 7148.
[16] J. Akola, K. Rytkonen, M. Manninen, *J. Phys. Chem. B* **2006**, *110*, 5186 – 5190.
[17] a) H. Isla, M. Gallego, E. M. Pérez, R. Viruela, E. Ortí, N. Martín, *J. Am. Chem. Soc.* **2010**, *132*, 1772 – 1773; b) D. Canevet, M. Gallego, H. Isla, A. de Juan, E. M. Pérez, N. Martín, *J. Am. Chem. Soc.* **2011**, *133*, 3184 – 3190.
[18] C. Romero-Nieto, R. García, M. Á. Herranz, C. Ehli, M. Ruppert, A. Hirsch, D. M. Guldi, N. Martín, *J. Am. Chem. Soc.* **2012**, *134*, 9183 – 9192.
[19] R. H. Grubbs, *Tetrahedron* **2004**, *60*, 7117 – 7140.
[20] The fact that larger macrocycles do not necessarily lead to a higher degree of functionalization is in agreement with our previous findings on the association of fullerenes by related macrocycles. We have shown that small changes in the structure of the receptor often lead to changes in the association constant of several orders of magnitude.[17b]
[21] S. M. Bachilo, M. S. Strano, C. Kittrell, R. H. Hauge, R. E. Smalley, R. B. Weisman, *Science* **2002**, *298*, 2361 – 2366.
[22] E. Nakamura, *Angew. Chem.* **2013**, *125*, 248 – 266; *Angew. Chem. Int. Ed.* **2013**, *52*, 236 – 252.
[23] M. Koshino, T. Tanaka, N. Solin, K. Suenaga, H. Isobe, E. Nakamura, *Science* **2007**, *316*, 853.

  